Bioactive Materials 8 (2022) 109–123

Contents lists available at ScienceDirect

Bioactive Materials

journal homepage: www.sciencedirect.com/journal/bioactive-materials

Nanoporous titanium implant surface promotes osteogenesis by suppressing osteoclastogenesis via integrin β1/FAKpY397/MAPK pathway

Yide He [a,1], Zhe Li [a,1], Xin Ding [a,b,1], Boya Xu [a], Jinjin Wang [c], Yi Li [a], Fanghao Chen [a], Fanhui Meng [d,**], Wen Song [a,*], Yumei Zhang [a,***]

[a] State Key Laboratory of Military Stomatology & National Clinical Research Center for Oral Diseases & Shaanxi Key Laboratory of Oral Diseases, Department of Prosthodontics, School of Stomatology, The Fourth Military Medical University, Xi'an, China
[b] Huaian Stomatological Hospital, Nanjing, China
[c] State Key Laboratory of Military Stomatology & National Clinical Research Center for Oral Diseases & Shaanxi Key Laboratory of Oral Diseases, Department of Periodontology, School of Stomatology, The Fourth Military Medical University, Xi'an, China
[d] State Key Laboratory of Military Stomatology, Department of Dental Materials, School of Stomatology, The Fourth Military Medical University, Xi'an, Shaanxi, China

ARTICLE INFO

Keywords:
Nanoporous implant
Osteogenesis
Osteoclastogenesis
FAK phosphorylation
MAPK

ABSTRACT

Macrophages and osteoclasts are both derived from monocyte/macrophage lineage, which plays as the osteoclastic part of bone metabolism. Although they are regulated by bone implant surface nanoarchitecture and involved in osseointegration, the beneath mechanism has not been simultaneously analyzed in a given surface model and their communication with osteoblasts is also blurring. Here, the effect of implant surface topography on monocyte/macrophage lineage osteoclastogenesis and the subsequent effect on osteogenesis are systematically investigated. The nanoporous surface is fabricated on titanium implant by etching and anodizing to get the nanotubes structure. The early bone formation around implant is significantly accelerated by the nanoporous surface in vivo. Meanwhile, the macrophage recruitment and osteoclast formation are increased and decreased respectively. Mechanistically, the integrin mediated FAK phosphorylation and its downstream MAPK pathway (p-p38) are significantly downregulated by the nanoporous surface, which account for the inhibition of osteoclastogenesis. In addition, the nanoporous surface can alleviate the inhibition of osteoclasts on osteogenesis by changing the secretion of clastokines, and accelerate bone regeneration by macrophage cytokine profiles. In conclusion, these data indicate that physical topography of implant surface is a critical factor modulating monocyte/macrophage lineage commitment, which provides theoretical guidance and mechanism basis for promoting osseointegration by coupling the osteogenesis and osteoclastogenesis.

1. Introduction

With the popularization of orthopedic implant, rapid establishment and maintaining the stability of osseointegration are of crucial important to ensure the success rate [1]. Instead of merely exploring the osteogenesis behaviors around bone implant, the role of monocyte/macrophage lineage cells has attracted more and more attention in recent years due to their regulatory potency for osseointegration [2]. Briefly, after implant surgery, the monocyte/macrophage lineage cells are the first to reach the surgical site and contact with implant surface through local microcirculation [3]. The macrophages (Mϕs) are not only important for innate immune response, but also play dominant role in bone homeostasis via polarizing into M1/M2 states to coordinate the communication with osteoblasts [4]. Previously, studies have confirmed the macrophage polarization shift induced by TiO_2 nanotubular surfaces [5,6]. We have also investigated effects of micropitted/nanotubular titania topographies on macrophage polarization and have confirmed their contribution to osseointegration [7–9]. However, the

Peer review under responsibility of KeAi Communications Co., Ltd.
* Corresponding author.
** Corresponding author.
*** Corresponding author.
E-mail addresses: mngfanhui@163.com (F. Meng), songwenfmmu@hotmail.com (W. Song), wqtzym@fmmu.edu.cn (Y. Zhang).
[1] Equal contribution.

https://doi.org/10.1016/j.bioactmat.2021.06.033
Received 12 May 2021; Received in revised form 22 June 2021; Accepted 27 June 2021
Available online 1 July 2021

monocyte/macrophage lineage is highly dynamic and diverse. In particular, its downstream osteoclasts (OCs), recently known as a kind of niche-specific tissue resident macrophages, are not only account for bone resorption, but also coupling with osteogenesis by secreting clastokines [10]. Therefore, the regulation mechanism of osteoclast differentiation from monocyte/macrophage lineage by implant surface nanoarchitecture should not be neglected. In addition, the comparison between upstream macrophages and downstream osteoclasts has not been investigated in one system.

In fact, the influence of implant surface topography on osteoclastogenesis has already been observed. However, the conclusions are often controversial. For example, some reported that the osteoclast formation is inhibited on roughed surface, whereas some others reported the reversed findings [11–13]. A crucial reason may be that the beneath regulation mechanism has not been elucidated yet. In general, the osteoclasts are formulated from the receptor activator of nuclear factor-kappa B ligand (RANKL) stimulated monocyte-macrophage, which is defined by the presence of at least three nuclei and positive tartrate-resistant acid phosphatase (TRAP) expression [14]. Since the osteoclasts are differentiated from monocyte/macrophage lineage in the presence of RANKL, we infer that there might be some shared mechanisms between the macrophage polarization and osteoclastogenesis regulation. Focal adhesion is a well-organized organelle composed of proteins including integrin, talin, vinculin, etc., connecting the cytoskeleton to extracellular matrix and mediating signal transduction [15,16]. From the transmembrane integrin protein to intracellular focal adhesion kinase (FAK) is a well-accepted bridge to link the intracellular responses with external stimuli, particularly the substrate physical information such as stiffness and topography. Previously our group has confirmed that the physical topography on titanium surface has a significant effect on the polarization determination of macrophages through FAK mediated mitogen activated protein kinase (MAPK) signaling activation [9]. The induction of osteoclasts via RANKL-RANK axis is also mediated by MAPK signaling [17]. Moreover, it is reported that the substrate topography will refine the FA organization and thus influencing the sealing zone of osteoclasts [12,18]. Consequently, it is reasonable to deduce that the FAK may be involved in the osteoclast formation from monocyte-macrophage. Taken together, we hypothesized that the implant surface topography may influence the osteoclastogenesis via the FAK-MAPK pathway.

The regulation effect of monocyte/macrophage lineage secretion products on osteogenesis is rather sophisticate and has not been fully elucidated yet. In the macrophage stage, the secreted cytokines are dependent on polarization status. In brief, the M1 polarized macrophages secret proinflammatory cytokines, while the M2 type macrophages mainly secret prohealing cytokines, which are conducive to osteogenesis [3]. In the osteoclast stage, the various products secreted by osteoclasts have been defined as clastokines, which could be classified into positive and negative regulators of osteogenesis [19]. Therefore, in order to find out how monocyte/macrophage lineage regulating bone regeneration, the whole spectrum of both cytokines from macrophages and clastokines from osteoclasts needs to be comprehensively analyzed.

In the present study, the nanoporous surface was fabricated by anodizing of Ti surface to generate the titania nanotubular structure. The effect of implant nanotopography on the distribution of macrophages and osteoclasts was observed by histological study in vivo. The murine monocyte-macrophage cell line RAW264.7 was subjected to RANKL treatment to induce osteoclastogenesis on different surfaces. The findings confirmed that nanoporous surface could inhibit osteoclast formation through integrin mediated FAK phosphorylation and its downstream MAPK pathway, especially p38. The secretion productions of monocyte/macrophage lineage cells were fully investigated and the differentially expressed cytokines could significantly benefit bone regeneration.

2. Materials and methods

2.1. Ti samples preparation and characterization

Commercially pure Ti (99.9%, Grade 1) disks (diameter = 15 mm, thickness = 1.5 mm, in vitro section) and rods (diameter = 1 mm, length = 2 mm, in vivo section) were provided by Northwest Institute for Nonferrous Metal Research, Xi'an, China. Then, both the disks and the rods were polished from 400 to 7000 meshes and washed sequentially in acetone, ethanol and deionized water to generate the polished Ti (PT) surface. The micropitted topography (MT) was obtained on the PT surface by etching in 0.5 wt% hydrofluoric acid for 30 min. The micropit-nanotube topography (MNT) was prepared on the MT surface according to our previous study [9,20]. In brief, the MT samples were respectively anodized in an electrolyte (0.5 wt% hydrofluoric acid and 1 M phosphoric acid) at 5 V (MNT5), 10V (MNT10), 15V (MNT15) and 20V (MNT20) for 60 min at room temperature to generate nanotube arrays with gradient diameter. Then the annealing treatment was carried out at 450 °C for 3 h. The surface morphology was observed by a field-emission scanning electron microscope (FE-SEM; Hitachi S-4800) while the topography was scanned by an atomic force microscope (AFM; Shimadzu). The DSA1 System (Krüss) was used to measure the surface water contact angle to assess the hydrophilicity of the samples. All samples were sterilized with 75% ethanol and ultraviolet irradiation.

2.2. In vivo assessment of osteogenesis and osteoclastogenesis around Ti implants

2.2.1. Animal surgery

In this section, the prepared Ti rods (25 for each group) with different surfaces (PT and MNT5) were implanted into the femur metaphysis of 25 male mice (average body weight = 24 g, 8-week-old). All animal procedures were performed according to guidelines approved by the University Research Ethics Committee of the Fourth Military Medical University. In brief, the mice were anesthetized and the surgical areas of the mice were shaved and disinfected. Then the femur metaphysis was carefully exposed via skin incision and muscle dissection. A hole of 1 mm in diameter was prepared on the metaphysis of each femur using a fissure bur. Two Ti rods with different topographies (PT and MNT5) were implanted into the predrilled holes in each mouse (one rod per femur). Finally, muscles and skins were sutured severally with absorbable sutures, and the surgical area was disinfected again. The mice were sacrificed after 1, 3, 5, 7 and 14 days and femurs containing implants were obtained and fixed in 4% paraformaldehyde.

2.2.2. Micro-computed tomography (micro-CT) scanning

All femur samples collected on the 14th day after implantation were detected using a micro-CT scanner (YXLON International GmbH). The results were analyzed via VGStudio Max 2.2 (Volume Graphic). A cylindrical area surrounding the implant with a diameter of 300 μm and a length of 2 mm was defined as the region of interest (ROI). The new bone volume ratio (bone volume to total volume, BV/TV), trabecular numbers (TbN), trabecular thickness (TbTh), and trabecular separation (TbSp) of samples of each group were calculated.

2.2.3. Immunohistochemical/immunofluorescent staining and TRAP staining

After micro-CT scanning, the femur samples were decalcified in 10% EDTA (Sigma) for 3 weeks. After decalcification treatment, the Ti rods were easily removed from femurs without destroying the bone tissue around the implant. Then the samples were dehydrated by serial ethanol and embedded in paraffin. Serial cross sections (4 μm thick) were obtained using a microtome (Leica RM2235), followed by immunohistochemical and immunofluorescent staining of OPN and F4/80 respectively. TRAP staining was performed by using the Acid Phosphatase Leukocyte Kit (Sigma). The detailed information of antibodies was

listed in Table S1. After mounting on coverglass, the samples were imaged by optical microscope (Olympus) and confocal laser scanning microscope (CLSM, Olympus). The images were analyzed quantitatively by Fiji software.

2.3. In vitro assessment of osteoclast differentiation

2.3.1. Cell culture

The RAW264.7 cells were purchased from ATCC company. To induce osteoclast (OC) differentiation, the cells were seeded at a density of 2×10^4 cells/well on the Ti samples placed in 24 well plates, cultured in Dulbecco's modified Eagle's medium (DMEM, Gibco, Grand Island, NY, USA) containing 10% fetal bovine serum (FBS; HyClone), 2 mM L-glutamine, 1% penicillin-streptomycin (HyClone) and 20 ng/mL RANKL (Peprotech, Rocky Hill, NJ, USA) for 4 days.

2.3.2. TRAP staining

TRAP staining was conducted using the Acid Phosphatase Leukocyte Kit (Sigma) according to the manufacturer's instructions. Briefly, osteoclasts were fixed with fixative solution (25 mL Citrate Solution, 65 mL acetone and 8 mL of 37% formaldehyde) for 30 s and stained with acid phosphatase solution (900 μL of deionized water, 40 μL of acetate solution, 10 μL of naphthol AS-BI phosphoric acid, 10 μL of tartrate solution, and 20 μL of diazotized Fast Garnet GBC per 1 ml of acid phosphatase solution) for 1 h in 37 °C protected from light. Then the cells were counterstain in hematoxylin solution for 2 min and rinsed several minutes in water. The samples were imaged immediately by using stereomicroscope (Leica).

2.3.3. TRAP activity assay

An Acid Phosphatase Assay Kit (Abcam) was used to determine TRAP activity. Briefly, after washed with PBS, cells were rinsed with 100 μL of the assay buffer and centrifuge 3 min at 4 °C at 13,000 rpm to remove any insoluble material and collect supernatant. The 4-nitrophenyl phosphate was dissolved in the assay buffer to prepare substrate solution. Samples of each group were added to substrate solution and incubated at 37 °C protected form light. At the same time, the standard solution (substrates containing acid phosphatase enzyme) and sample background solution (samples without substrates) were prepared. At the end of the reaction time, the reaction was discontinued by adding stop solution and the absorption was measured at 405 nm to calculate the value of TRAP activity.

2.3.4. The mRNA level of osteoclastogenic markers

The total RNA was extracted from osteoclasts with TRIzol reagent (Takara) to perform the real-time quantitative polymerase chain reaction (RT-qPCR). Mouse complementary DNA (cDNA) was reverse-transcribed from the total RNA with using the PrimeScript™ RT reagent kit (TaKaRa) and amplified using TB Green® Premix Ex TaqTM II (Takara). The mRNA expressions of cathepsin K (CTSK), matrix metalloproteinase-9 (MMP9), TRAP and receptor activator of nuclear factor κB (RANK) were normalized to Glyceraldehyde 3-phosphate dehydrogenase (GAPDH). The primers used in this section are listed in Table S2.

2.3.5. The protein level of osteoclastogenic markers

Osteoclastogenesis-related proteins were assayed by western blot. Cells were harvested and lysed using RIPA Lysis Buffer (Beyotime) supplemented with protease/phosphatase inhibitor cocktail (CST). Protein concentrations were determined with bicinchoninic acid assay (Beyotime). After equalized protein extracts were boiled, proteins were separated by sodium dodecyl sulfate-polyacrylamide gel electrophoresis (SDS-PAGE) and electophoretically transferred to polyvinylidene fluoride (PVDF) membranes. The membranes were then incubated with specific antibodies against CTSK, TRAP and GAPDH and developed to show the protein of interest. The detailed information of each antibody is showed in Table S1. Semi-quantitative measurements were performed using Fiji software.

2.4. Cell morphology and cytoskeleton observation

The methods of cell seeding and inducing osteoclast differentiation were the same to section 2.3.1. For the cell morphology observation, the cells were washed twice with PBS, fixed with 2.5% glutaraldehyde at 4 °C overnight, and dehydrated by ethanol (30, 50, 70, 80, 90, and 100 vol %). After vacuum drying using hexamethyldisilazane (HMDS), the cells were sputter-coated with platinum and observed by FE-SEM (Hitachi S-4800). For the cytoskeleton staining, the cells were washed twice with PBS, fixed with 4% PFA for 20 min and permeabilized by 0.1% Triton X-100 for 5 min. Then the cells were blocked with 1% bovine serum albumin (BSA) for 30 min. After washing twice, the samples were labeled with integrin αV antibody and Alexa Fluor 635-conjugated secondary antibody. Meanwhile, Alexa Fluor 488 phalloidin (Invitrogen) and Hoechst 33342 (Thermo Fisher Scientific) were used to stain F-action and nucleus respectively. Related antibodies were listed in Table S1. After mounted with ProLong Glass Antifade Mountant (Invitrogen), the cells were subjected to CLSM examination. Five scopes of each sample were randomly selected and the representative images were provided. The osteoclast area and the number of nuclei per cell were calculated with Fiji software.

2.5. Integrin-FAK-MAPK pathway regulation

After inducing osteoclast differentiation for 4 days according to the method mentioned in section 2.3.1, LC-MS/MS analysis was carried out. Concretely, osteoclast samples were sonicated three times on ice using a high intensity ultrasonic processor (Scientz) in lysis buffer (8 M urea, 1% protease inhibitor cocktail) and centrifuged at 12 000 g at 4 °C for 15 min to remove debris. For digestion, the protein solution was reduced with 5 mM dithiothreitol for 30 min at 56 °C and alkylated with 11 mM iodoacetamide for 15 min at room temperature in darkness. The protein sample was diluted by adding 100 mM triethylammonium bicarbonat to urea concentration less than 2 M and trypsin was added for digestion. Then peptide was desalted by Strata X C18 SPE column (Phenomenex) and vacuum-dried. Peptide was reconstituted in 0.5 M TEAB and processed according to the manufacturer's protocol for TMT kit/iTRAQ kit. After that, the tryptic peptides were fractionated into fractions by high pH reverse-phase highperformance liquid chromatography (HPLC) using Thermo Betasil C18 column and then concentrated and freeze dried for LC-MS. The tryptic peptides were dissolved in solvent A (0.1% formic acid and 2% acetonitrile) and were then separated in an EASY-NLC 1000 ultra-HPLC system. After separation, protein peptides were subjected to an NSI ion trap for ionization and were then analyzed in Q ExactiveTM Plus (Thermo Fisher Scientific). The ion trap setting was 2.0 kV. An Orbitrap instrument with high resolution of 70,000 was employed for detection and analysis. The resulting data were processed using Maxquant software [21]. Protein expression was considered significantly different when $p < 0.05$ and fold changes (FC) for differentially expressed proteins $> |1.2|$. Data visualization and volcano plots was performed with Graphpad Prism 8. ClusterProfiler was used for gene ontology (GO) enrichment analysis [22]. GO terms were evaluated using the online database Gene Ontology Consortium tool (AmiGo; http://geneontology.org).

For further testing, osteoclast protein lysates were extracted and integrin/FAK signaling and MAPK signaling pathway (p-JNK, total-JNK, p-p38, total-p38, p-ERK1/2 and total-ERK1/2) were detected by western blot. In order to further explore the role of FAK and p38 phosphorylation in osteoclast differentiation influenced by nanotopography, 5 μmol/L p-FAK (Tyr397) inhibitor (Defactinib hydrochloride, MedChemExpress) or 1 μmol/L p-p38 inhibitor (PD169316, MedChemExpress) was added to the culture medium during inducing osteoclast differentiation for 4 days and the protein expression of FAK phosphorylation of tyrosine 397

(FAKpY397), total-FAK, CTSK and TRAP was examined by western blot. The bands were captured by Tanon-5500 (Shanghai, China) and analyzed by ImageJ software. The antibodies used in this section are presented in Table S1.

2.6. Influence of clastokines on osteogenic differentiation

After inducing osteoclast differentiation according to the method in section 2.3.1, fresh α-MEM medium containing 10% FBS and 1% penicillin-streptomycin was used for continued culture for 2 days and the supernatant was collected every day. The supernatant of each group was diluted 1:1 in the osteogenic medium (OM, α-Minimal Essential Medium (α-MEM, Gibco) supplemented with 10% FBS, 20 mM β-glycerophosphate (Sigma), 100 mg/mL ascorbic acid (Sigma) and 2×10^{-7} M dexamethasone (Sigma)) before use and denoted as PT/osteoclast-conditioned medium (PT/OC-CM) and MNT5/OC-CM according to the topography of Ti samples. The conditioned medium (CM) was used for inducing osteogenic differentiation of MC3T3-E1 cells on tissue culture polystyrene (TCPS). MC3T3-E1 on TCPS cultured with standard osteogenic medium (α-MEM containing 10% FCS, 10 mM β-glycerophosphate, 50 mg/mL ascorbic acid and 1×10^{-7} M dexamethasone) without CM was used as blank control.

After culturing for 4 days, RT-qPCR analysis was used to detect the mRNA expression of osteogenic genes such as osteocalcin (OCN), osteopontin (OPN), alkaline phosphatase (ALP) and Runt-related transcription factor 2 (RUNX2). After culturing for 14 days, ALP activity and extracellular matrix (ECM) mineralization were analyzed using ALP staining and Alizarin Red S (ARS) staining respectively, following manufacturer's instructions. The images were analyzed semi-quantitatively using Fiji software. Furthermore, the gene expression of nine clastokines, including bone morphogenetic protein 6 (Bmp6), cardiotrophin-1 (CT-1), collagen triple helix repeat containing 1 (Cthrc1), hepatocyte growth factor (Hgf), slit guidance ligand 3 (Slit3), sphingosine kinase 1 (Sphk1), Wnt10b, sclerostin (Scl) and semaphorin4d (Sema4d), after cell culturing for 4 days on different surfaces were quantified using RT-qPCR. All primers used in this section are listed in Table S2. At the same time, the cell culture supernatant from each group was collected and the concentrations of Scl and Hgf were detected using a Mouse Scl ELISA Kit (Elabscience) and a Mouse HGF ELISA Kit (R&D Systems) according to the manufacturer's instructions.

2.7. Influence of macrophages secretions on osteogenic differentiation

After culturing the RAW264.7 cells on the PT or MNT5 surface for 4 days, fresh α-MEM medium was used for continued culture for 2 days and the supernatant was collected every day. The subsequent methods of indirect co-culture and osteogenesis test were the same as section 2.6. To identify the phenotype of macrophages, the cytokine profiles of macrophages supernatant were analyzed using Mouse Cytokine Array C2000 (Ray Biotech) according to the manufacturer's protocol. The intensities of signals were quantified by densitometry. Raw intensities were revised by background and normalized by median. FC in protein expression were calculated ($FC > |1.2|$ and $p < 0.05$ was considered significantly different). Cluster analysis and biological process GO terms identified by GO enrichment analysis were visualized according to differentially expressed cytokines.

2.8. Statistical analysis

Experiments were performed at least three times to ensure consistent results. All images were randomly obtained from samples. The statistical analysis was conducted using GraphPad Prism 8.0 software. Experimental data were assessed using one-way analysis of variance (ANOVA) followed the Tukey post hoc test or using a two-tailed Student's *t*-test (as appropriate). Differences were considered to be statistically significant when p values were less than 0.05.

3. Results

3.1. Characterizations of implant surface

The different topographies were examined by FE-SEM. The PT exhibited a smooth surface (Fig. 1A). Micro-pits etched by hydrofluoric acid could be observed on the MT and MNT surface under lower magnification (Fig. S1). The porous structure with about 30, 50, 70 and 100 nm diameters was respectively fabricated on the MNT5, MNT10, MNT15 and MNT20 surface, which could be examined under higher magnification. (Figs. 1A and S2). The water contact angle was about 67° for PT and about 24° for MNT5, indicating the significantly increased hydrophilicity of the MNT5 surface (Fig. 1B). The topography and the Sq roughness were measured by AFM. The MNT5 surface fluctuated homogeneously with ~11 folds higher roughness compared to the PT surface (Fig. 1C and D).

3.2. The osteogenesis was enhanced on the MNT5 surface in vivo

In order to assess the effect of physical pattern on osteogenesis, the early-stage osteogenic inductivity of different implant surfaces was dynamically evaluated in vivo (Fig. S2). The immunohistochemistry and immunofluorescence at 3, 7 and 14 days after implantation demonstrated that the expression of OPN, an important bone matrix protein, was significantly upregulated by the MNT5 surface (Fig. 2A and B). The semi-quantitative evaluation of immunohistochemical staining indicated that the OPN expression was significantly upregulated as early as day 7 (Fig. 2C). Moreover, micro-CT scanning indicated that the implant coated with MNT5 possessed better osseointegration with higher BV/TV and TbN and lower TbSp compared to the PT group, although the TbTh had no significant difference between the two groups (Fig. 2D–H). These results indicates that nanostructured implants of possess greater osteogenic inductivity.

3.3. The macrophage infiltration and osteoclast formation were promoted and inhibited respectively on the MNT5 surface in vivo

Since monocyte/macrophage lineage cells have the ability to regulate osteogenic behavior, the macrophage distribution was detected by immunohistochemistry and immunofluorescence staining of F4/80, the macrophage surface marker. The F4/80 positive cells were detected on both surfaces during the early-stage of implant-host interaction at different observation times (Fig. 3A and B). The semi-quantitative evaluation of F4/80 immunohistochemical staining indicated that the macrophage infiltration was increased at first and then decreased, and the infiltration number was more on the MNT5 surface (Fig. 3D).

Furthermore, the distribution of osteoclasts around implants was determined by the immunohistochemistry of TRAP staining. On day 1 after implantation, it is difficult to find osteoclasts in bone tissue around both implants. On day 3, a small amount of osteoclasts could be observed and the MNT5 implant showed more osteoclasts than the PT implant. On day 5, the TRAP positive osteoclasts became obvious adjacent to implant surface, and the MNT5 implant showed less osteoclasts than the PT implant. On day 7, the number of osteoclasts was decreased in both implants and there were still more osteoclasts in the PT group compared to the MNT5 group (Fig. 3C). The semi-quantitative evaluation indicated that the TRAP positive osteoclasts both increased at first and then decreased rapidly, and the MNT5 surface showed more rapid emerging and vanishing of osteoclasts and the osteoclasts number was generally lower (Fig. 3E). Therefore, nanostructured implants can recruit more macrophages and inhibit osteoclast formation in vivo.

3.4. Osteoclastogenic differentiation was inhibited on the MNT5 surface

From the above observations, the monocyte/macrophage system was indeed influenced by different implant surface topographies. In order to

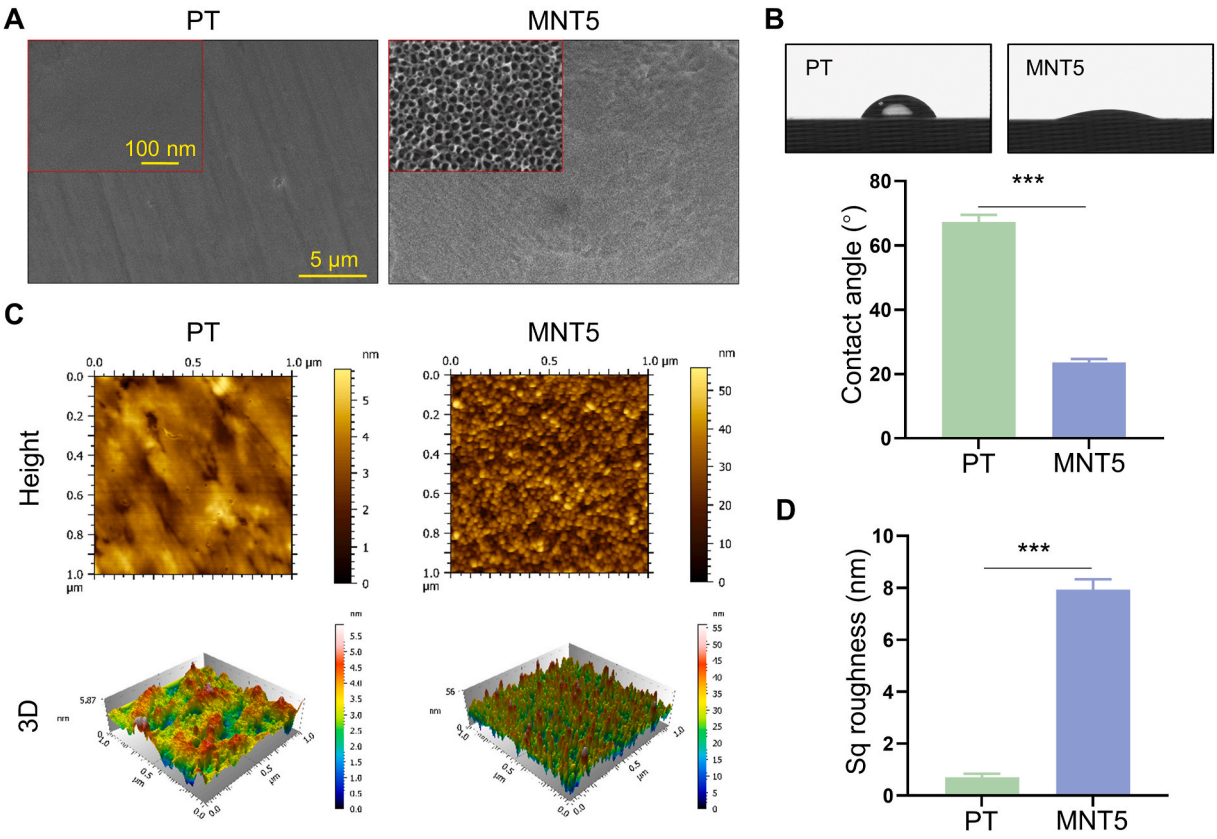

Fig. 1. Implant surface characterizations. A) FE-SEM observation. B) Water contact angle measurement. C) Top view and 3D of surface height fluctuations of AFM scanning images. D) Surface Sq roughness. PT, the polished Ti; MNT5, the micropit-nanotube fabricated by etching and anodizing at 5V. Data are presented as mean ± SEM, n = 3, Student's *t*-test, ***P < 0.001.

verify the effect of surface topography on osteoclastogenic differentiation of monocyte/macrophage, TRAP staining was performed after RANKL induction for 4 days. The brown staining spots represented positive osteoclasts and the number of osteoclasts were evidently decreased on the MNT5 surface (Fig. 4A). Meanwhile, the TRAP activity of osteoclasts was significantly inhibited on the MNT5 surface (Fig. 4B). Furthermore, the gene expression of osteoclastogenic markers were checked. The expression of CTSK, MMP9 and TRAP was decreased on the MNT5 surface (Fig. 4C–E), though the RANK gene expression showed no significant difference between the two groups (Fig. 4F). Similarly, the protein expression of CTSK and TRAP was also reduced in osteoclasts in the MNT5 group confirmed by western blot (Fig. 4G–I). The formulated osteoclasts were observed by FE-SEM. Compared to the PT surface, the osteoclasts morphology on the MNT5 surface was much smaller (Fig. 4M). The actin staining showed a typical podosome belt (known as actin ring) corresponding to many F-actin columns arranged at the peripheral area of osteoclasts on the PT surface (Fig. 4J). However, there were few multinucleuated cells on the MNT5 surface, and the actin ring size was also much smaller (Fig. 4J). Quantitative assessment manifested that the relative cell area and the number of nuclei on the MNT5 surface were significantly decreased (Fig. 4K and L). These observations point to the fact that nanopatterned titanium surface could inhibit osteoclastogenic differentiation in cell morphology, number and activity.

To further study the relationship between nanotubes diameter and osteoclast differentiation, a series size of MNT (from MNT5 to MNT20) were used to culture and induce osteoclasts. Compared with PT and MT group, the number of TRAP positive spots on MNT surface was significantly reduced (Fig. S3A). The quantitative results of TRAP activity showed that compared with the polished surface, the appearance of micro-pits could inhibit osteoclast differentiation (Fig. S3B). In addition, the inhibitory effect of osteoclast differentiation was further enhanced after the nanotube arrays were modified on the micro-pits with dependence on the size of nanotubes. Nanotubes with larger diameter possessed stronger the inhibitory effect on osteoclastogenesis (Fig. S3B). The expression of osteoclast marker genes (MMP9 and TRAP) was decreased with the increase of the diameter of nanotubes (Fig. S4). Immunofluorescence staining further confirmed the above phenomenon. The osteoclasts on the polished surface were large and typical, but there were few osteoclasts with more than three nuclei on the MNT surface, especially MNT20 (Fig. S5).

3.5. *The osteoclast differentiation was inhibited by MNT5 surface via focal adhesion*

To uncover the regulation mechanism behind the osteoclastogenic inhibition on the MNT5 surface, the proteomic profiling of osteoclasts was checked by LC-MS/MS analysis. 5307 proteins containing quantitative information were detected in total and the corresponding proteomic profiles of osteoclasts on the PT and MNT5 surface are presented in volcano plots (Fig. 5A). Among the proteins of the MNT5 group, 27 proteins were upregulated and 52 proteins were downregulated compared to the PT group. GO enrichment analysis further revealed that differentially expressed proteins were mainly related to cell adhesion functions (Fig. 5B). The GO terms were classified into biological process (BP), cellular component (CC) and molecular function (MF) and ranked by enrichment factor [-log10(p value)]. Given the fact that the surface nanostructure directly affects the cell adhesion, the components of focal adhesion complex was examined in detail by western blot. There was no significant difference in the expression of integrin αV and integrin β3 between the two groups, but the integrin β1 expression was decreased in osteoclasts on the MNT5 surface compared to the PT surface (Fig. 5C and

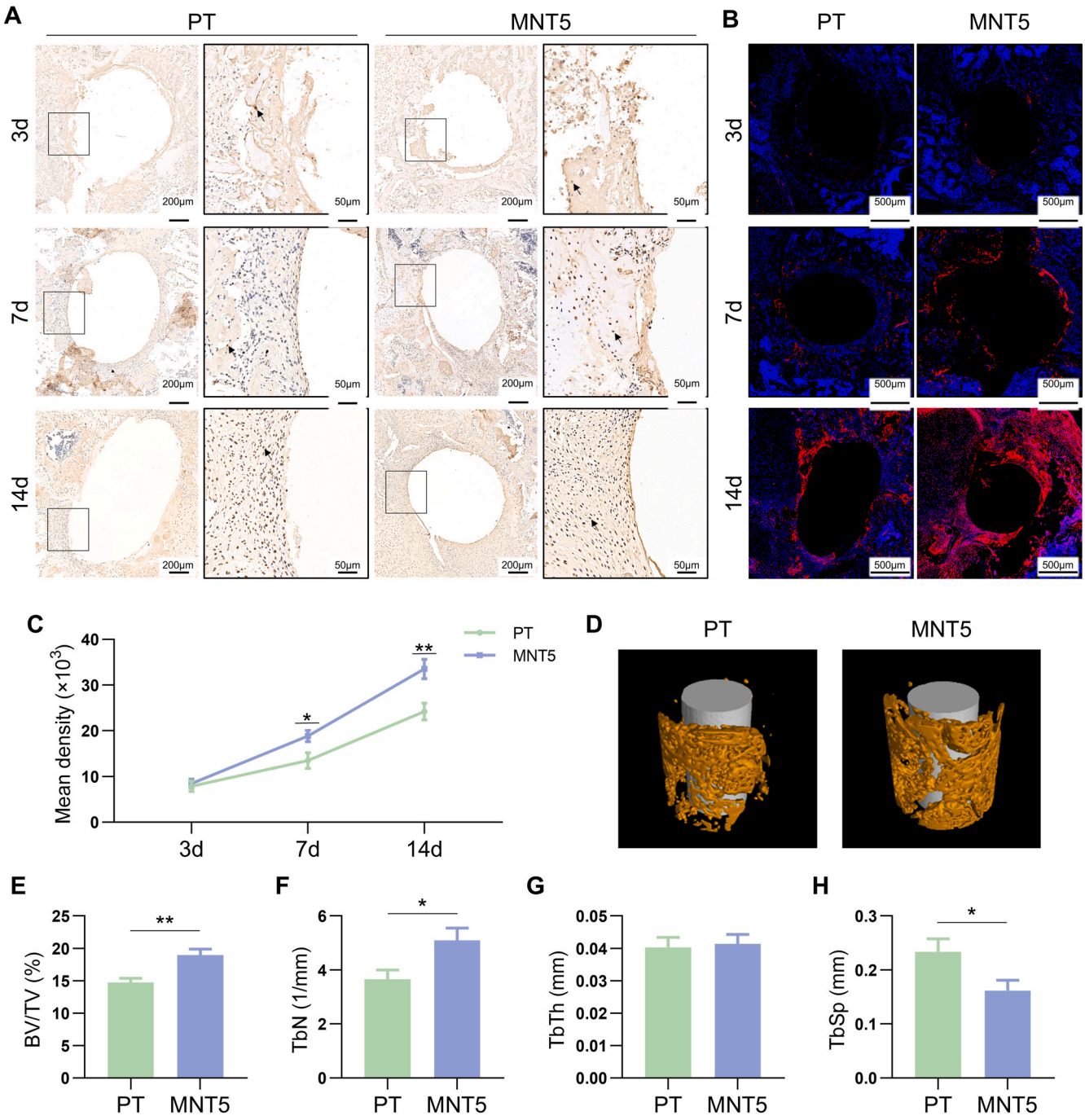

Fig. 2. The early-stage osteogenesis around implant surface. A) Immunohistochemistry staining of OPN indicates bone regeneration on implant surface. Arrow heads represent positive expression. The framed images in the right column are the magnified box area in the left column. B) Immunofluorescence staining of OPN in peri-implant tissue. Red indicates positive expression, blue indicates cell nucleus. C) Semi-quantitative analysis of OPN immunohistochemistry staining. D) 3D reconstruction of micro-CT data depicts new bone formation. E,F,G,H) Quantifications of BV/TV, TbN, TbTh and TbSp in the ROI of micro-CT data, respectively. n = 5 male mice for 3, 7 and 14 day after implantation operation, respectively. Data are presented as mean ± SEM, n = 5, Student's *t*-test, *P < 0.05, **P < 0.01. (For interpretation of the references to colour in this figure legend, the reader is referred to the Web version of this article.)

D). Furthermore, the expression of FAKpY397 was evidently decreased on the MNT5 surface and twice as low as that on the PT surface (Fig. 5E and F). When osteoclasts were treated with p-FAK (Tyr397) inhibitor, the expression of FAKpY397 was further inhibited. Meanwhile, the expression of osteoclast marker proteins (CTSK and TRAP) of each group was decreased correspondingly (Fig. 5G and H). These results demonstrate that the MNT5 topography inhibit osteoclast differentiation through inhibiting the expression of integrin β1 and FAK phosphorylation.

Furthermore, the MAPK pathway was measured, which was known as the downstream of FAK phosphorylation. Compared to the PT surface, the phosphorylation levels of JNK and p38 on the MNT5 surface was significantly decreased and the phosphorylation levels of ERK1/2 was evidently increased (Fig. 5I–K). In addition, the inhibition of FAK phosphorylation caused further decrease of p-p38 (Fig. S6). When cells were treated with p-p38 inhibitor, the expression of osteoclastogenic marker TRAP was decreased (Fig. S6). Therefore, the decrease of FAK phosphorylation of MNT5 group led to the change of MAPK pathway,

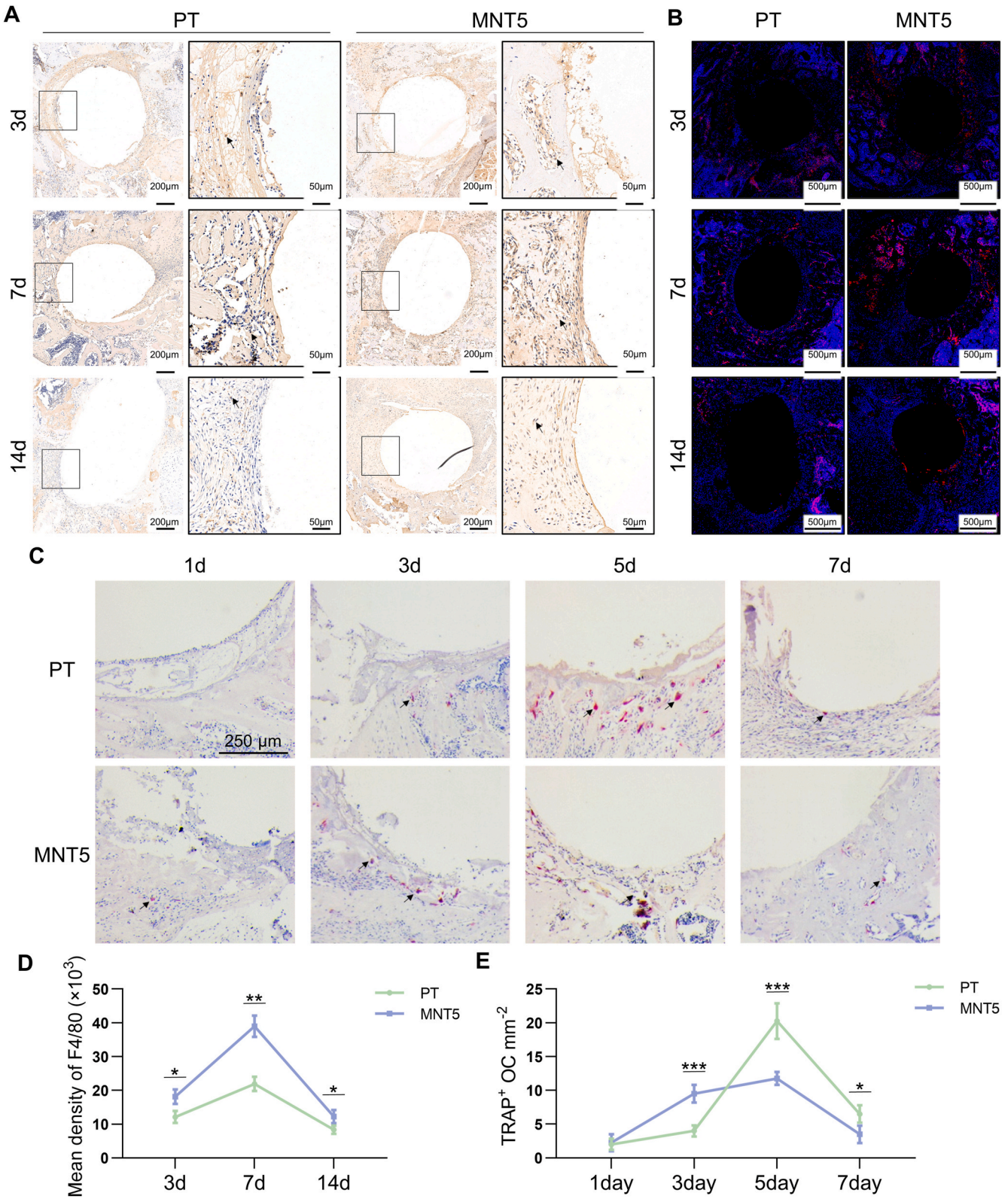

Fig. 3. The monocyte/macrophage infiltration and osteoclastogenesis during early-stage of implant-host interaction. A) Immunohistochemistry staining of F4/80 marks macrophages in peri-implant tissue. Arrow heads indicate positive expression. The framed images in the right column are the magnified box area in the left column. B) The immunofluorescence staining of F4/80. Red indicates positive expression, blue indicates cell nucleus. C) TRAP staining marks osteoclasts in peri-implant tissue. Arrow heads indicated positive cells. D) Semi-quantitative analysis of F4/80 immunohistochemistry staining. E) Semi-quantitative analysis of TRAP staining. n = 5 male mice for 1, 3, 5, 7, 14 day after implantation operation, respectively. Data are presented as mean ± SEM, n = 5, Student's *t*-test, *P < 0.05, **P < 0.01, ***P < 0.001. (For interpretation of the references to colour in this figure legend, the reader is referred to the Web version of this article.)

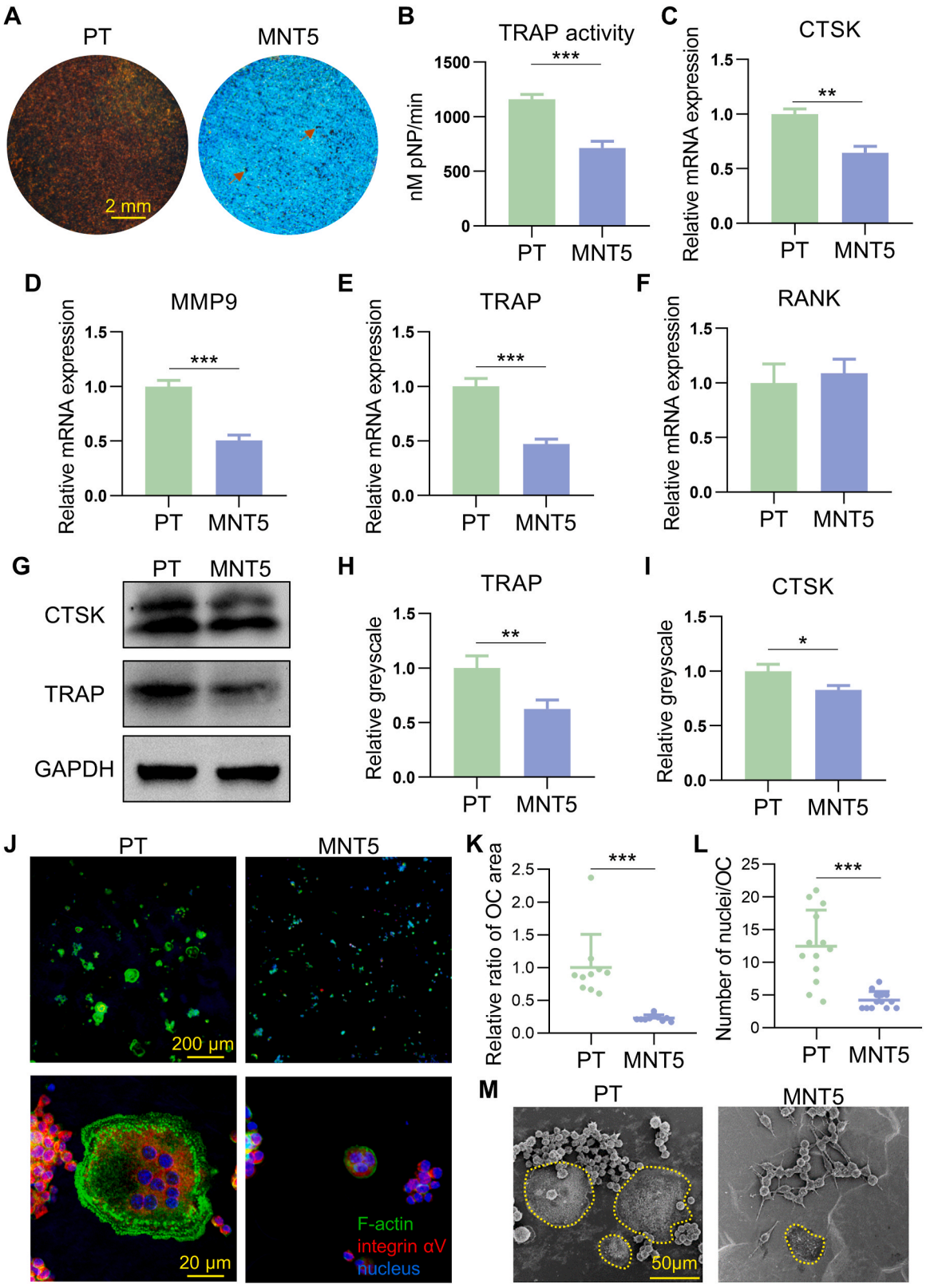

Fig. 4. The osteoclast differentiation and cell morphology of monocyte/macrophage on different surfaces. A) The TRAP staining marks mature osteoclasts on the titanium with different surfaces after culturing for 4 days. B) TRAP activity assay of osteoclasts. C,D,E,F) The osteoclastogenic genes (CTSK, MMP9, TRAP and RANK) expression determined by RT-qPCR. G,H,I) Western blot analysis of CSTK and TRAP expression and semi-quantification. J) Immunofluorescence staining depicts the actin ring structure of osteoclasts on different surfaces after culturing for 4 days. K,L) The relative cell area and nucleus number of matured osteoclasts on both surfaces. M) FE-SEM observation of matured osteoclasts on different surfaces. Yellow curves indicate the multinucleated osteoclasts. Data are presented as mean ± SEM, n = 3, Student's *t*-test, *P < 0.05, **P < 0.01, ***P < 0.001. (For interpretation of the references to colour in this figure legend, the reader is referred to the Web version of this article.)

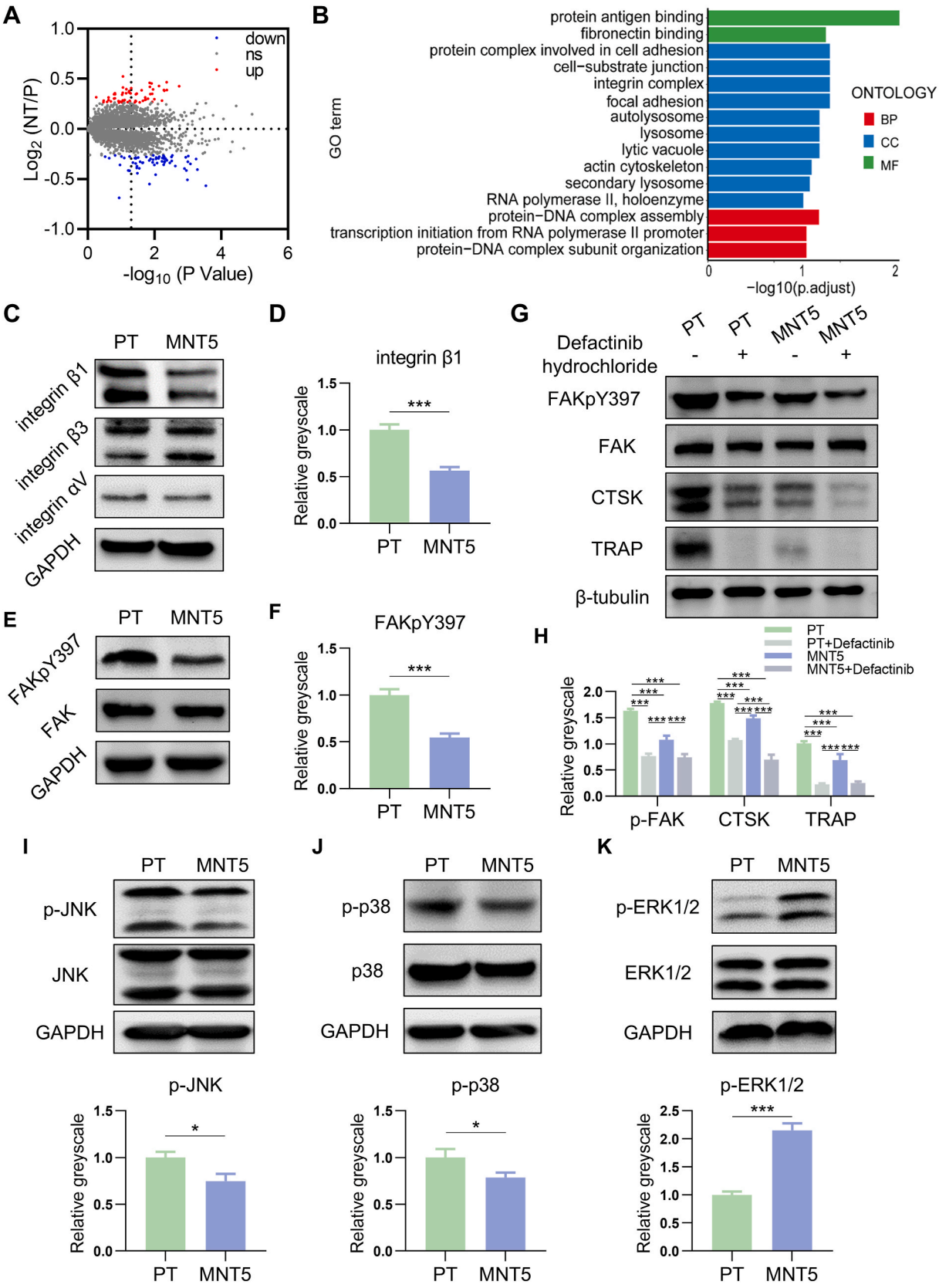

Fig. 5. Mechanism analysis of osteoclast differentiation regulated by different surfaces. A) LC-MS/MS proteomic analysis are presented in volcano plots. (Student's *t*-test). B) GO enrichment analysis of differential proteins. (Student's *t*-test). C,D,E,F) Western blot of integrin β1, integrin β3, integrin αV, FAKpY397 and FAK expression in osteoclasts and semi-quantification compared to GAPDH expression. (Student's *t*-test). G,H) The identification of the role of FAK phosphorylation in osteoclast differentiation by western blot. (One-way ANOVA). I,J,K) Phosphorylation of JNK, p38 and ERK1/2 detected by western blot and semi-quantification compared to GAPDH expression. (Student's *t*-test). Data are presented as mean ± SEM, n = 3, *P < 0.05, ***P < 0.001.

and the reduced expression of p38 phosphorylation inhibited the osteoclast differentiation.

3.6. The osteogenesis was inhibited by clastokines, which was partially alleviated by MNT5 surface

In consideration of the regulation of osteoclasts on osteoblasts, the osteogenic ability of MC3T3-E1 with exposure to OC-CM that obtained from different surfaces were assessed by RT-qPCR, ALP as well as ARS staining analysis (Fig. 6A). Compared to the OC-CM obtained from the PT surface, the expression of osteogenic genes including OPN and RUNX2 in osteoblasts were upregulated by the OC-CM that obtained from the MNT5 surface (Fig. 6C, E). The ALP production and ECM mineralization were also promoted by the OC-CM from the MNT5 surface (Fig. 6F). However, the OC-CM from both PT and MNT5 showed significant inhibition of the osteogenesis of MC3T3-E1 compared to the standard OM (Fig. 6B–F). This indicated that the osteoclasts secretions have negative effect on bone regeneration and the MNT5 surface could partially alleviate the inhibition. To elucidate how osteoclasts regulate osteoblasts, nine reported clastokines expression was quantified by RT-qPCR. The expression of Bmp6, Cthrc1, Hgf, Slit3 and Wnt10b, which promote osteogenesis, was upregulated on the MNT5 surface compared to the PT surface. In particular, the expression of Bmp6, Hgf and Wnt10b was upregulated at least 3 times and the Slit3 expression was upregulated about 28.5 times in the MNT5 group. Besides, the expression of Scl and Sema4d, which inhibit bone formation, was significantly

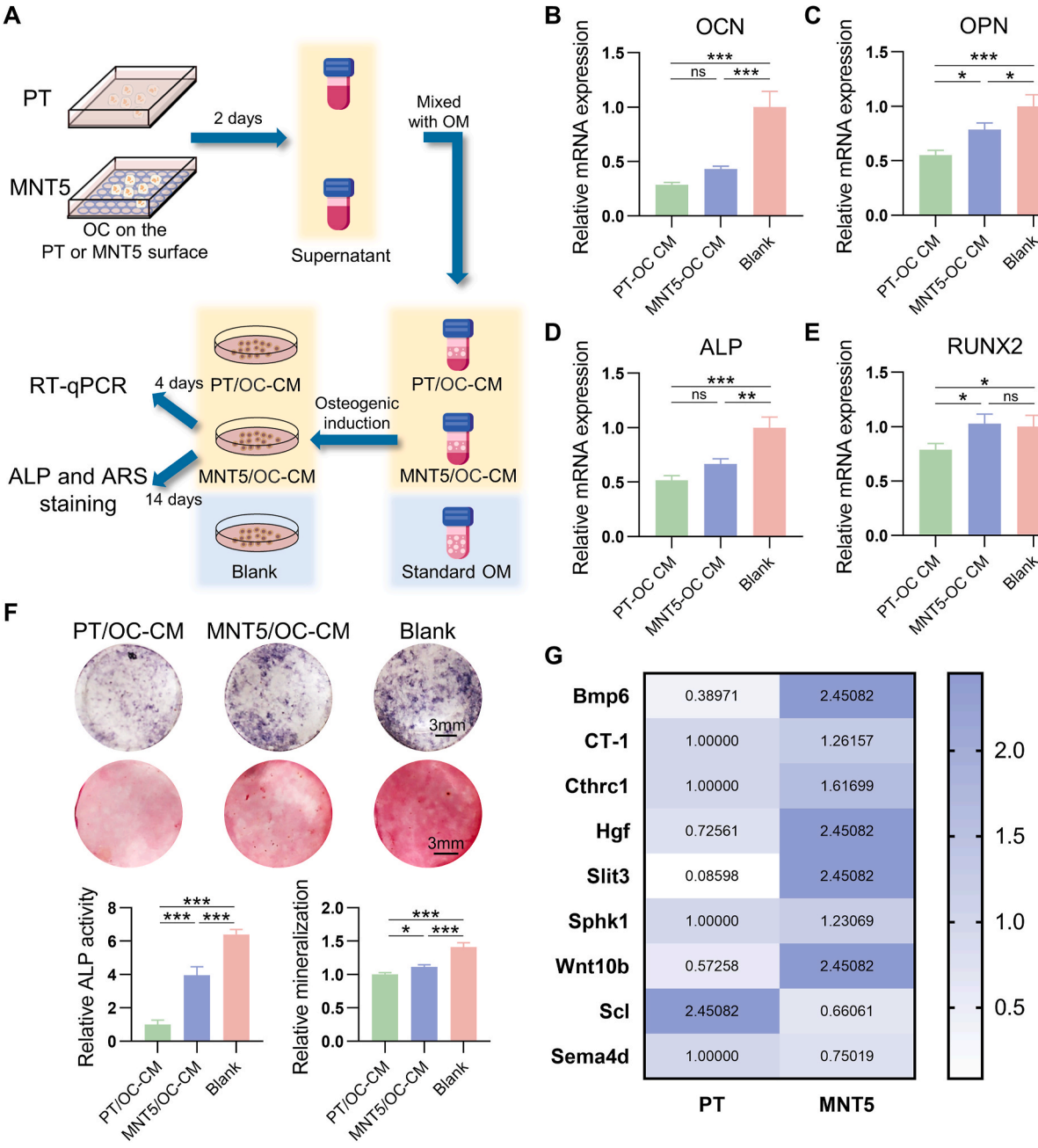

Fig. 6. Effect of osteoclast conditioned medium on osteogenesis of osteoblasts. A) Schematic illustration of experimental procedure. B,C,D,E) The expression of osteogenic genes including OCN, OPN, ALP and RUNX2 of osteoblasts determined by RT-qPCR. (One-way ANOVA). F) ALP staining and ARS staining of osteoblasts. G) The expression of clastokines of osteoclasts on different titanium surfaces determined by RT-qPCR. (Student's *t*-test). Data are presented as mean ± SEM, n = 3, *P < 0.05, **P < 0.01, ***P < 0.001, ns = no significance.

downregualted in the osteoclasts on the MNT5 surface (Fig. 6G). In order to further explore whether only the MNT5 surface has the ability to regulate the expression of clastokines, the effect of gradient diameter nanotubes on the secretion of Scl and Hgf was examined by ELISA. the MNT surface promoted Hgf expression and inhibited Scl expression compared to the PT and MT surface (Fig. S7). In particular, the MNT5 surface with about 30 nm nanotubes had the strongest ability to regulate the secretion profiles of clastokines to promote osteogenesis among the nanotubes with different diameters (Fig. S7). Taken together, osteoclasts on the nanoporous titanium surface can reduce the inhibition of osteogenesis through secreting clastokines.

3.7. The osteogenesis was promoted by Mϕ cytokines, which was further enhanced by MNT5 surface

To comprehensively understand the control of monocyte/macrophage lineage on osteoblasts, the osteogenic regulatory role of CM from macrophages was analyzed. In contrast to osteoclasts, CM from macrophages greatly promoted osteogenic differentiation. RT-qPCR results showed that the expression of osteogenic marker gene in osteoblasts in the blank control was the lowest; the expression of OCN, ALP and Runx2 in osteoblasts regulated by MNT5/Mϕ-CM was higher than that regulated by PT/Mϕ-CM (Fig. 7A–D). Therefore, macrophages on the MNT5 surface have stronger osteogenic induction ability than the PT surface. This trend was also confirmed by ALP and ARS staining results (Fig. 7E). In order to find out the reason, a detailed analysis of the cytokine profiles from macrophages on different surfaces was performed by cytokine arrays. Among 144 secretory proteins detected, 8 were upregulated and 11 were downregulated in the macrophages on the MNT5 surface (Fig. 7F). Most of the upregulated cytokines were related to the prohealing (M2) phenotype of macrophage and the downregulated cytokines mostly belonged to expression profiles of proinflammatory (M1) macrophages (Table S3). Functional enrichment analysis of the differentially expressed cytokines showed in Fig. 7g. The upregulated proteins induced by nanotopography were related to cell differentiation and proliferation, osteogenesis and angiogenesis, and the regulation of MAPK cascade and protein phosphorylation. Meanwhile, the downregulated proteins were mainly associated with response to tumor necrosis factor, regulation of calcium ion transport and inflammatory response. At the same time, both upregulated and downregulated proteins were annotated with cell adhesion and migration (Fig. 7G). These data demonstrate that nanoporous surface on titanium surface can modulate macrophages toward anti-inflammatory and prohealing phenotypes and promote bone regeneration by changing a series of macrophage-derived cytokine secretion.

Taken together, the monocyte/macrophage lineage cells are all regulated by implant surface nanoarchitecture, which contribute to osteogenesis in different ways. Specifically, in the macrophages stage, the Mϕ secreted cytokines are beneficial for osteogenesis, in which the proinflammatory and prohealing cytokines are down- and up-regulated by the MNT5 surface respectively. During the differentiation from macrophages to osteoclasts, the osteoclasts formation is inhibited by MNT5 surface via blocking integrin mediated FAK phosphorylation and downstream MAPK pathway. In the osteoclasts stage, the clastokines are impeding for osteogenesis, in which the pro-osteogenesis and anti-osteogenesis cytokines are up- and down-regulated by MNT5 surface respectively (Fig. 8).

4. Discussion

Nanostructure of implant surface can significantly regulate the behavior of surrounding monocytic lineage-derived cells, thus affecting bone healing. In this study, we have confirmed that nanoporous titanium implants have better osseointegration, which is due to promoting the recruitment of macrophages around the implants and limiting the differentiation and chemotaxis of osteoclasts. The nanoporous topography could induce macrophages to transform into anti-inflammatory phenotype and alter the secretion of cytokines, thus promoting the mineralization of osteoblasts. In the meanwhile, the nanotopography can significantly inhibit the differentiation of osteoclasts through integrin β1/FAKpY397 signaling pathway, block cell extension, and change the secretion level of clastokines, thus alleviating the inhibition of osteogenesis from osteoclasts.

A variety of nanopatterns on implant surface can contribute to the process of osseointegration, which may be due to the changes in the distribution and phenotype of the monocyte/macrophage lineage cells. For example, Karazisis et al. found that relatively fewer CD68-positive macrophages were recruited in the tissue surrounding the nanoscaled implants compared with the polished surface [23]. We systematically observed the distribution of monocytic lineage-derived cells around the implant in the early stage of implantation. In general, compared with the PT surface, the MNT5 surface was more conducive to recruit macrophages and inhibit subsequent osteoclast differentiation. Osteoclasts and macrophages showed the opposite distribution trend on the two different topographies. The reason may be that macrophages and osteoclasts are two competing differentiation outcomes from myeloid progenitors [24]. Given that the different roles of macrophages and osteoclasts in bone remodeling, the functional balance between these two types of cells may be particularly important.

Bone resorption by osteoclasts is a complex process including cytokine-mediated osteoclast differentiation and homing, osteoclast adhesion to specific sites on the bone surface and the generation of resorptive units, which is regulated at multiple levels in time and space [11]. Osteoclasts can perceive various characteristics of extracellular matrix through their integrin and focal adhension, including the chemical properties, degree of mineralization, local rigidity and topography of matrix [25]. Osteoclasts manifest polarized morphology with sealing zone to absorb bone tissue and show spread morphology with no specific actin structures to migrate [26]. The sealing zone is a unique large band consists of a central ring of actin filaments and the inner and outer rings of integrin and other adhesion proteins on both sides [27]. Once the actin ring/sealing zone is formed, osteoclasts could start appropriate bone resorption [28]. In addition, the size of osteoclast, including cell area and the number of nuclei, is also an index to measure the bone resorption activity of osteoclast. The larger the osteoclasts are, the more resorption lacunae they can produce [29]. Through morphological observation, we found that the osteoclasts on the MNT5 surface hardly showed actin rings which obviously appeared on the PT surface, and the cell area and the number of nuclei/cell were less than that on the PT surface. Furthermore, we confirmed that the inhibition of osteoclast differentiation enhanced with the increase of nanotube diameter. Therefore, the nanotopography we fabricated on the titanium surface inhibits osteoclast differentiation.

A variety of nanotopographies have been confirmed to have the ability to regulate osteoclast differentiation, but there is still no unified understanding concerning the regular pattern of different surface roughness. Studies indicated that osteoclast fusion and resorptive activity were impeded by micro-nanostructured hydroxyapatite materials compared to smooth surface, which was partly associated with disruption of actin rings [12,13]. We also found that both micro/-nanotopography could significantly lower osteoclast TRAP activity and gene expression of osteoclastogenic markers compared to the polished or micropitted surface, which may be attributed to the synergy effect of micro/nano roughness. However, some reports showed that large and stable actin rings of osteoclasts were found on the smooth surfaces made of calcite crystals with 12 nm roughness, and small and unstable actin rings were appeared on rough calcite crystals with 530 nm roughness. The same tendency was also demonstrated on the surface of glass substrate [11]. Gross et al. confirmed that sprayed hydroxyapatite coating could induce much stronger absorption activity of osteoclasts compared to polished hydroxyapatite coating [30]. The reason for the divergence of topographical regulation may be the inconsistency of culture

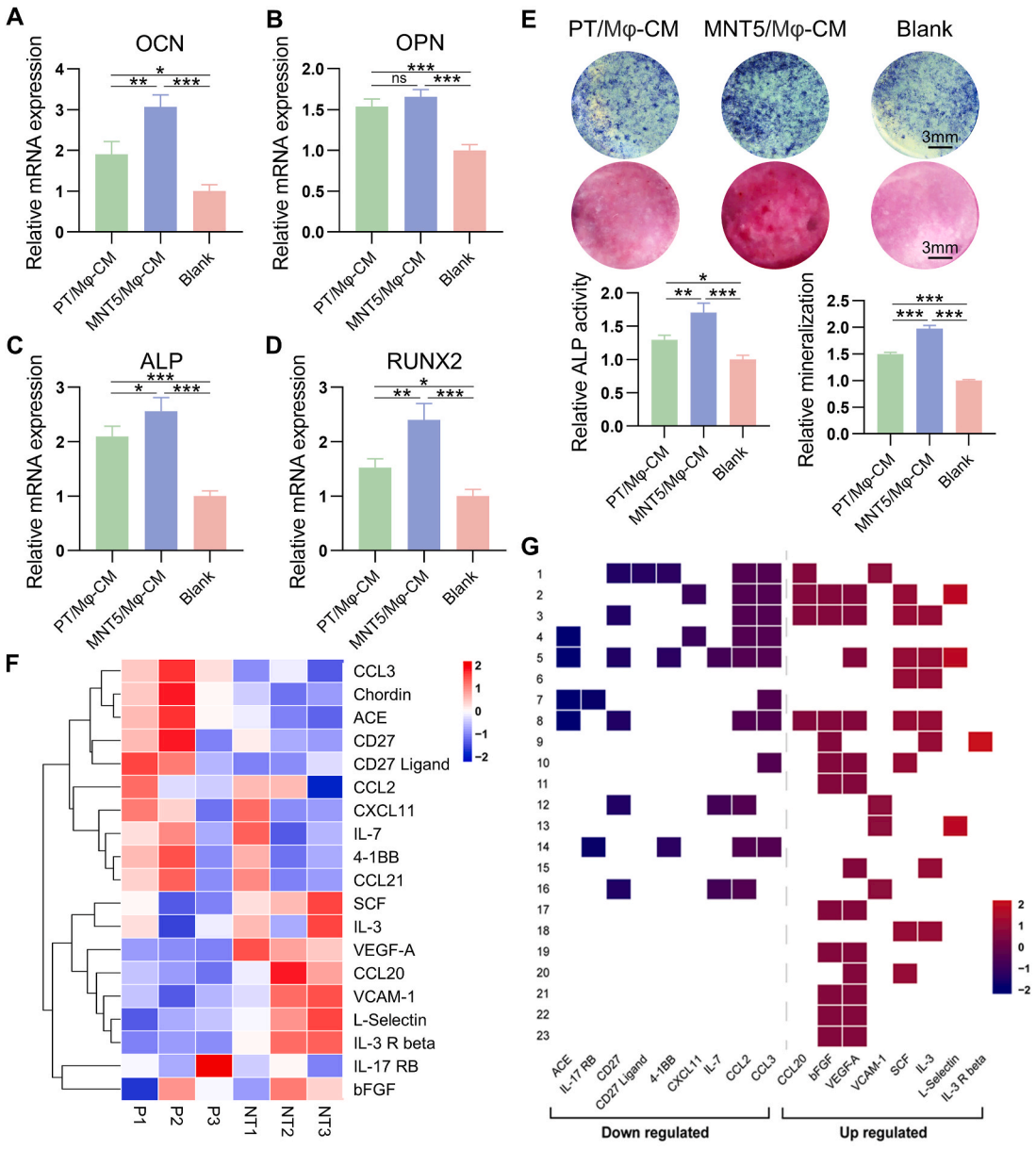

Number	Term	Number	Term
1	cellular response to tumor necrosis factor	13	leukocyte tethering or rolling
2	positive regulation of cell migration	14	regulation of protein transport
3	regulation of MAPK cascade	15	monocyte differentiation
4	regulation of calcium ion transport	16	positive regulation of cell−cell adhesion
5	regulation of apoptotic process	17	blood vessel endothelial cell migration
6	regulation of mast cell proliferation	18	regulation of myeloid cell apoptotic process
7	positive regulation of inflammatory response	19	positive regulation of sprouting angiogenesis
8	regulation of protein phosphorylation	20	positive regulation of stem cell proliferation
9	peptidyl−tyrosine phosphorylation	21	positive regulation of DNA biosynthetic process
10	regulation of protein kinase B signaling	22	positive regulation of osteoblast differentiation
11	positive regulation of endothelial cell chemotaxis	23	mucopolysaccharide metabolic process
12	positive regulation of T cell activation		

Fig. 7. Effect of macrophage conditioned medium on osteogenesis of osteoblasts. A,B,C,D) The expression of osteogenic genes including OCN, OPN, ALP and RUNX2 of osteoblasts determined by RT-qPCR. (One-way ANOVA). E) ALP staining and ARS staining of osteoblasts. F) Cluster analysis of differential cytokine profiles from macrophages on different surfaces measured by protein array. (Student's *t*-test, FC > 1.2 or FC < 1/1.2). G) The heatmap-like functional classification of the differential cytokines. X-axis represents differential cytokines sorted by fold change (MNT5:PT). Y-axis represents top terms enriched in biological process. Data are presented as mean ± SEM, n = 3, *P < 0.05, **P < 0.01, ***P < 0.001, ns = no significance.

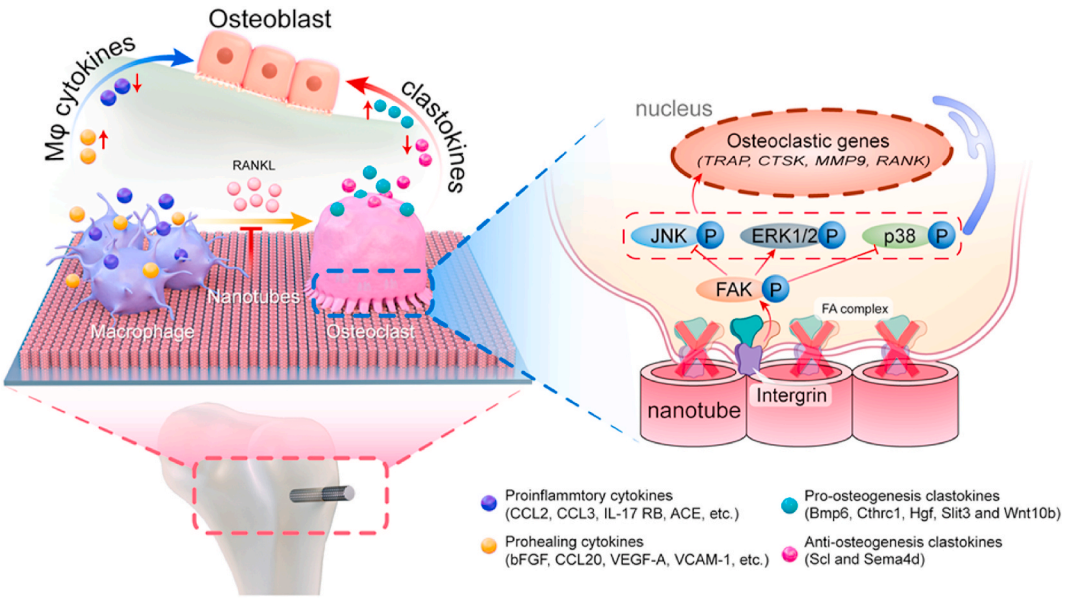

Fig. 8. A schematic diagram depicting the role of the MNT5 surface in promoting osteogenesis by modulating monocyte/macrophage lineage.

conditions and time, and the complexity of substrate perception of cells.

The effect of substrate topography on osteoclast behaviour depends on the adhesion-mediated surface perceptive ability and elucidating the cellular mechanism triggered by them is important not only for understanding the bone resorption and remodeling process, but also for designing and manufacturing implant materials with good bone compatibility and osseointegration. Biomaterial surfaces are known to influence the formation of focal adhesions, the key structure mediating cell adhesion [31,32]. The number of focal adhesions is decreased when cells are cultured on micro/nano-topography in comparison to flat substrates [33]. For osteoclasts, RANKL-mediated osteoclastogenesis requires the activation of its receptor integrin β1 [34]. We used proteomics and western blot to analyze related protein expression and found that integrin β1 was downregulated in osteoblasts on the MNT5 surface. Integrin αVβ3 is identified as the dominant binding domain of osteoclasts and particularly rich at podosomes, responsible for recognizing ligands of the ECM and regulating cell interaction with the ECM [28,35,36]. However, some studies claimed that the lack of integrin αVβ3 has little inhibitory effect on osteoclast differentiation [37]. Our results showed that there was no significant difference in the integrin αV and integrin β3 expression of osteoclasts on the two different titanium surfaces, at least indicating that the nanotopography we prepared has a selective inhibition effect on the subunit of integrin. Moreover, we found that the MNT5 surface reduce the phosphorylation level of FAK tyrosine 397 of osteoclasts and the addition of p-FAK (Tyr397) inhibitor further inhibit osteoclast differentiation. Therefore, the tyrosine 397 phosphorylation of FAK is necessary for physiological osteoclast formation [38]. The MAPK pathway is one of the important signaling events downstream of FAK [39]. Therefore, we also detected the expression of MAPK pathway, which could activate the downstream positive regulators of osteoclast differentiation [40]. The expression of p-JNK and p-p38 was inhibited and the p-ERK1/2 expression was promoted in osteoclasts cultured on the MNT5 surface. Among the three MAPKs, p38 has been proved to play an essential role in mediating osteoclast differentiation [17,41]. We found that the inhibition of p-FAK impeded the p38 phosphorylation and the inhibition of p-p38 further inhibited osteoclast differentiation. Considering the inhibitory effect of MNT5 on osteoclast differentiation, our results are consistent with previous studies that the phosphorylation of p-p38 is favorable for osteoclastogenesis, while the phosphorylation of p-ERK1/2 is not [17,42]. In summary, we propose for the first time that titanium surface nanotopography hinders osteoclast differentiation through inhibiting the expression of integrin β1/FAKpY397 and further influencing MAPK cascade signaling. It may be due to the fact that porous nanostructures could not provide enough cell adhesion sites and hamper the pivotal osteoclast migration and fusion.

It is believed that both macrophages and osteoclasts can manipulate osteogenesis by secreting a variety of cytokines [43]. In order to identify the topography induced regulation of bone formation by monocytic lineage-derived cells, we used CM to induce mineralization of osteoblasts in vitro. Interestingly, we found that CM from macrophages could promote bone formation, while CM from osteoclasts could inhibit it. Compared with the PT surface, CM from macrophages on the MNT5 surface had more obvious promoting effect and the osteoclastic CM had less inhibitory effect on osteogenesis. We further examined the cytokine secretion of macrophages and osteoclasts. In the upregulated cytokines, fibroblast growth factor (bFGF) and chemokine ligand 20 (CCL20) could promote macrophage polarization toward a M2 phenotype [44,45]. Moreover, increased vascular endothelial growth factor-A (VEGF-A), vascular cell adhesion molecule-1 (VCAM-1) and L-selectin could induce cell ingress to the fracture site, couple angiogenesis and osteogenesis and promote bone healing [46–49]. On the other hand, the downregulated CCL2, CCL3, CCL21, C-X-C motif chemokine 11 (CXCL11), IL-17 RB (Interleukin-17 receptor B) and angiotensin-converting enzyme (ACE) belong to M1 polarization secretion spectrum of macrophages [3,50–54]. Because IL-7 could promote IL-17-mediated bone loss and Chordin is a critical inhibitor of the BMPs signaling pathway, decreased IL-7 and Chordin are beneficial to bone protection [55,56]. CD27 Ligand, markedly expressed on Th1 cells, is required for Th1-type immune responses and its downregulated secretion is helpful to reduce the inflammatory reaction [57]. Functional enrichment analysis further proved that the changed cytokine secretion could contribute to stem cell differentiation, bone tissue regeneration and angiogenesis, and inhibit the progress of inflammatory response. These may be due to the regulation of cell adhesion and migration caused by physical topographical factors. Adhesion plaque acts as a sensor to sense the alterations of substrates, which causes the rearrangement of cytoskeleton and finally touches off a series of biological effects through the changes of MAPK and other signaling pathways [58].

Although cytokine expression profiles we here show can explain the way of macrophages regulating bone regeneration on the different topographies to a certain extent, it is difficult to simulate the real situation

in vivo by cell culture because macrophage has strong plasticity and its phenotype and function is constantly changing in the whole dynamic process of bone remodeling. Loi et al. studied the impact of sequential modulation of macrophage phenotype on pre-osteoblast mediated bone formation in vitro: All of the main macrophage phenotypes including M0, M1 and M2 promoted MC3T3-E1 mediated bone formation in direct co-culture [59]. It may be due to the fact that osteoblasts in direct co-culture system can also act on macrophages and change their final phenotype.

Clastokines, serving as the coupling factors, are secreted by osteoclasts and regulate the behavior and recruitment of osteoblasts [19,60]. Some clastokines could recruit osteoblasts and promote bone matrix deposition and mineralization, including Bmp6, CT-1, Cthrc1, Hgf, Slit3, Sphk1 and Wnt10b [60–66]. Other clastokines such as Scl and Sema4d have the function of suppressing bone formation [67,68]. We found that the stimulation of nanotopography could promote the expression of a variety of pro-osteogenic clastokines, and significantly inhibit the expression of clastokines that promote bone resorption. In the osteoclasts on the MNT5 surface, the most obvious increase in gene expression was Slit3, which has an osteoprotective role through simultaneously regulate both bone formation and resorption [65]. Besides, we detected the expression of SCL and HGF of osteoclasts on nanotubes with gradient diameter (MNT5-MNT20) by ELISA and found that MNT5 have the strongest effect on promoting the expression of HGF and inhibiting the expression of SCL. Although we found that nanotubes with larger diameter, such as MNT20, have stronger ability to inhibit osteoclastic differentiation, it is not advisable to excessively inhibit osteoclast differentiation in order to promote osteogenesis. Moderate osteoclastic differentiation is beneficial to coupling osteogenesis [64]. Therefore, MNT5 is the more ideal nanotopography to promote bone regeneration.

Taken together, our findings indicate that the expression of clastokines from osteoclasts and cytokines from macrophages can be affected by the nanoporous titanium surface, and the changes of these secretory profiles are beneficial to accelerate the process of bone regeneration.

5. Conclusions

In this work, we systematically compared the effects of titanium surfaces with two topographies (MNT5 and PT) on the monocyte/macrophage lineage cells and their indirect regulation on bone formation. In vivo experiments showed that there were more macrophages and less osteoclasts around the MNT5 implant, and the bone healing rate was also faster. In vitro experiments confirmed that the nanoporous topography could significantly inhibit osteoclast differentiation through blocking integrin β1/FAKpY397/MAPK pathway, and alter the populations of clastokines and Mϕ cytokines to more osteogenesis favorable. These results indicate that the physical information of biomaterials surface is a crucial factor regulating implant osseointegration.

CRediT authorship contribution statement

Yide He: Conceptualization, Methodology, Investigation, Formal analysis, Data curation, Writing – original draft, Writing – review & editing. **Zhe Li:** Conceptualization, Methodology, Investigation, Resources, Data curation, Writing – original draft. **Xin Ding:** Conceptualization, Methodology, Investigation, Resources, Data curation, Writing – original draft, Writing – review & editing. **Boya Xu:** Methodology, Investigation, Formal analysis. **Jinjin Wang:** Methodology, Formal analysis. **Yi Li:** Methodology, Investigation. **Fanghao Chen:** Methodology, Investigation. **Fanhui Meng:** Methodology, Investigation, Supervision, Validation, Writing – review & editing, Project administration. **Wen Song:** Conceptualization, Supervision, Funding acquisition, Project administration, Writing – review & editing. **Yumei Zhang:** Conceptualization, Supervision, Funding acquisition, Project administration, Writing – review & editing.

Declaration of competing interest

The authors declare that they have no known competing financial interests or personal relationships that could have appeared to influence the work reported in this paper.

Acknowledgements

The work is supported by National Natural Science Foundation of China (81530051, 31800790 and 32071324) and Young Talent Fund of University Association for Science and Technology in Shaanxi, China (20190304).

Appendix A. Supplementary data

Supplementary data to this article can be found online at https://doi.org/10.1016/j.bioactmat.2021.06.033.

References

[1] M. Monjo, J.M. Ramis, H.J. Ronold, S.F. Taxt-Lamolle, J.E. Ellingsen, S. P. Lyngstadaas, Correlation between molecular signals and bone bonding to titanium implants, Clin. Oral Implants Res. 24 (9) (2013) 1035–1043.
[2] R.J. Miron, H. Zohdi, M. Fujioka-Kobayashi, D.D. Bosshardt, Giant cells around bone biomaterials: osteoclasts or multi-nucleated giant cells? Acta Biomater. 46 (2016) 15–28.
[3] J. Pajarinen, T. Lin, E. Gibon, Y. Kohno, M. Maruyama, K. Nathan, L. Lu, Z. Yao, S. B. Goodman, Mesenchymal stem cell-macrophage crosstalk and bone healing, Biomaterials 196 (2019) 80–89.
[4] A. Mantovani, S.K. Biswas, M.R. Galdiero, A. Sica, M. Locati, Macrophage plasticity and polarization in tissue repair and remodelling, J. Pathol. 229 (2) (2013) 176–185.
[5] W.P. Yu, J.L. Ding, X.L. Liu, G.D. Zhu, F. Lin, J.J. Xu, Z. Wang, J.L. Zhou, Titanium dioxide nanotubes promote M2 polarization by inhibiting macrophage glycolysis and ultimately accelerate endothelialization, Immun. Inflamm. Dis. (2021), https://doi.org/10.1002/iid3.429. In press.
[6] L.M. Chamberlain, K.S. Brammer, G.W. Johnston, S. Chen, S. Jin, Macrophage inflammatory response to TiO_2 nanotube surfaces, J. Biomaterials Nanobiotechnol. 2 (3) (2011) 293–300.
[7] Q.L. Ma, L.Z. Zhao, R.R. Liu, B.Q. Jin, W. Song, Y. Wang, Y.S. Zhang, L.H. Chen, Y. M. Zhang, Improved implant osseointegration of a nanostructured titanium surface via mediation of macrophage polarization, Biomaterials 35 (37) (2014) 9853–9867.
[8] J. Wang, F. Meng, W. Song, J. Jin, Q. Ma, D. Fei, L. Fang, L. Chen, Q. Wang, Y. Zhang, Nanostructured titanium regulates osseointegration via influencing macrophage polarization in the osteogenic environment, Int. J. Nanomed. 13 (2018) 4029–4043.
[9] Y. He, J. Luo, Y. Zhang, Z. Li, F. Chen, W. Song, Y. Zhang, The unique regulation of implant surface nanostructure on macrophages M1 polarization, Mater. Sci. Eng. C Mater. Biol. Appl. 106 (2020) 110221.
[10] M. Guilliams, G.R. Thierry, J. Bonnardel, M. Bajenoff, Establishment and maintenance of the macrophage niche, Immunity 52 (3) (2020) 434–451.
[11] D. Geblinger, L. Addadi, B. Geiger, Nano-topography sensing by osteoclasts, J. Cell Sci. 123 (Pt 9) (2010) 1503–1510.
[12] G. Ciapetti, G. Di Pompo, S. Avnet, D. Martini, A. Diez-Escudero, E.B. Montufar, M. P. Ginebra, N. Baldini, Osteoclast differentiation from human blood precursors on biomimetic calcium-phosphate substrates, Acta Biomater. 50 (2017) 102–113.
[13] D.O. Costa, P.D. Prowse, T. Chrones, S.M. Sims, D.W. Hamilton, A.S. Rizkalla, S. J. Dixon, The differential regulation of osteoblast and osteoclast activity by surface topography of hydroxyapatite coatings, Biomaterials 34 (30) (2013) 7215–7226.
[14] L.J. Raggatt, N.C. Partridge, Cellular and molecular mechanisms of bone remodeling, J. Biol. Chem. 285 (33) (2010) 25103–25108.
[15] H.Y. Lou, W. Zhao, X. Li, L. Duan, A. Powers, M. Akamatsu, F. Santoro, A. F. McGuire, Y. Cui, D.G. Drubin, B. Cui, Membrane curvature underlies actin reorganization in response to nanoscale surface topography, Proc. Natl. Acad. Sci. U. S. A. 116 (46) (2019) 23143–23151.
[16] P. Kanchanawong, G. Shtengel, A.M. Pasapera, E.B. Ramko, M.W. Davidson, H. F. Hess, C.M. Waterman, Nanoscale architecture of integrin-based cell adhesions, Nature 468 (7323) (2010) 580–584.
[17] K. Lee, Y.H. Chung, H. Ahn, H. Kim, J. Rho, D. Jeong, Selective regulation of MAPK signaling mediates RANKL-dependent osteoclast differentiation, Int. J. Biol. Sci. 12 (2) (2016) 235–245.
[18] A. Merolli, S. Fung, N.S. Murthy, E.T. Pashuck, Y. Mao, X. Wu, J.A.M. Steele, D. Martin, P.V. Moghe, T. Bromage, J. Kohn, Ruffled border" formation on a CaP-free substrate: a first step towards osteoclast-recruiting bone-grafts materials able to re-establish bone turn-over, J. Mater. Sci. Mater. Med. 29 (4) (2018) 38.
[19] A. Cappariello, A. Maurizi, V. Veeriah, A. Teti, The great beauty of the osteoclast, Arch. Biochem. Biophys. 558 (2014) 70–78.

[20] W. Wang, L. Zhao, K. Wu, Q. Ma, S. Mei, P.K. Chu, Q. Wang, Y. Zhang, The role of integrin-linked kinase/beta-catenin pathway in the enhanced MG63 differentiation by micro/nano-textured topography, Biomaterials 34 (3) (2013) 631–640.
[21] S. Tyanova, T. Temu, J. Cox, The MaxQuant computational platform for mass spectrometry-based shotgun proteomics, Nat. Protoc. 11 (12) (2016) 2301–2319.
[22] G. Yu, L.G. Wang, Y. Han, Q.Y. He, clusterProfiler: an R package for comparing biological themes among gene clusters, OMICS 16 (5) (2012) 284–287.
[23] D. Karazisis, S. Petronis, H. Agheli, L. Emanuelsson, B. Norlindh, A. Johansson, L. Rasmusson, P. Thomsen, O. Omar, The influence of controlled surface nanotopography on the early biological events of osseointegration, Acta Biomater. 53 (2017) 559–571.
[24] D. Yang, Y. Wan, Molecular determinants for the polarization of macrophage and osteoclast, Semin. Immunopathol. 41 (5) (2019) 551–563.
[25] K. Henriksen, D.J. Leeming, I. Byrjalsen, R.H. Nielsen, M.G. Sorensen, M. H. Dziegiel, T.J. Martin, C. Christiansen, P. Qvist, M.A. Karsdal, Osteoclasts prefer aged bone, Osteoporos. Int. 18 (6) (2007) 751–759.
[26] F. Saltel, O. Destaing, F. Bard, D. Eichert, P. Jurdic, Apatite-mediated actin dynamics in resorbing osteoclasts, Mol. Biol. Cell 15 (12) (2004) 5231–5241.
[27] P.T. Lakkakorpi, H.K. Vaananen, Cytoskeletal changes in osteoclasts during the resorption cycle, Microsc. Res. Tech. 33 (2) (1996) 171–181.
[28] K. Soe, J.M. Delaisse, X.G. Borggaard, Osteoclast formation at the bone marrow/bone surface interface: importance of structural elements, matrix, and intercellular communication, Semin. Cell Dev. Biol. 112 (2020) 8–15.
[29] R.L. Lees, J.N. Heersche, Macrophage colony stimulating factor increases bone resorption in dispersed osteoclast cultures by increasing osteoclast size, J. Bone Miner. Res. 14 (6) (1999) 937–945.
[30] K.A. Gross, D. Muller, H. Lucas, D.R. Haynes, Osteoclast resorption of thermal spray hydoxyapatite coatings is influenced by surface topography, Acta Biomater. 8 (5) (2012) 1948–1956.
[31] C.H. Seo, K. Furukawa, K. Montagne, H. Jeong, T. Ushida, The effect of substrate microtopography on focal adhesion maturation and actin organization via the RhoA/ROCK pathway, Biomaterials 32 (36) (2011) 9568–9575.
[32] Z. Li, Y. He, L.H. Klausen, N. Yan, J. Liu, F. Chen, W. Song, M. Dong, Y. Zhang, Growing vertical aligned mesoporous silica thin film on nanoporous substrate for enhanced degradation, drug delivery and bioactivity, Bioact. Mater. 6 (5) (2021) 1452–1463.
[33] M.J. Biggs, R.G. Richards, N. Gadegaard, C.D. Wilkinson, R.O. Oreffo, M.J. Dalby, The use of nanoscale topography to modulate the dynamics of adhesion formation in primary osteoblasts and ERK/MAPK signalling in STRO-1+ enriched skeletal stem cells, Biomaterials 30 (28) (2009) 5094–5103.
[34] X. Wang, W. Wei, J.Y. Krzeszinski, Y. Wang, Y. Wan, A liver-bone endocrine relay by IGFBP1 promotes osteoclastogenesis and mediates FGF21-induced bone resorption, Cell Metabol. 22 (5) (2015) 811–824.
[35] W. Zou, S.L. Teitelbaum, Absence of Dap12 and the alphavbeta3 integrin causes severe osteopetrosis, J. Cell Biol. 208 (1) (2015) 125–136.
[36] S.L. Teitelbaum, Osteoporosis and integrins, J. Clin. Endocrinol. Metab. 90 (4) (2005) 2466–2468.
[37] L. Kong, B. Wang, X. Yang, B. He, D. Hao, L. Yan, Integrin-associated molecules and signalling cross talking in osteoclast cytoskeleton regulation, J. Cell Mol. Med. 24 (6) (2020) 3271–3281.
[38] N. Kurio, T. Shimo, T. Fukazawa, M. Takaoka, T. Okui, N.M. Hassan, T. Honami, S. Hatakeyama, M. Ikeda, Y. Naomoto, A. Sasaki, Anti-tumor effect in human breast cancer by TAE226, a dual inhibitor for FAK and IGF-IR in vitro and in vivo, Exp. Cell Res. 317 (8) (2011) 1134–1146.
[39] Q. Li, Z. Wang, Involvement of FAK/P38 signaling pathways in mediating the enhanced osteogenesis induced by nano-graphene oxide modification on titanium implant surface, Int. J. Nanomed. 15 (2020) 4659–4676.
[40] S.K. Min, H.K. Kang, S.Y. Jung, D.H. Jang, B.M. Min, A vitronectin-derived peptide reverses ovariectomy-induced bone loss via regulation of osteoblast and osteoclast differentiation, Cell Death Differ. 25 (2) (2018) 268–281.
[41] J. Lin, D. Lee, Y. Choi, S.Y. Lee, The scaffold protein RACK1 mediates the RANKL-dependent activation of p38 MAPK in osteoclast precursors, Sci. Signal. 8 (379) (2015) ra54.
[42] H. Hotokezaka, E. Sakai, K. Kanaoka, K. Saito, K. Matsuo, H. Kitaura, N. Yoshida, K. Nakayama, U0126 and PD98059, specific inhibitors of MEK, accelerate differentiation of RAW264.7 cells into osteoclast-like cells, J. Biol. Chem. 277 (49) (2002) 47366–47372.
[43] Z. Chen, A. Bachhuka, F. Wei, X. Wang, G. Liu, K. Vasilev, Y. Xiao, Nanotopography-based strategy for the precise manipulation of osteoimmunomodulation in bone regeneration, Nanoscale 9 (46) (2017) 18129–18152.
[44] J. Wu, J. Zhu, Q. Wu, Y. An, K. Wang, T. Xuan, J. Zhang, W. Song, H. He, L. Song, J. Zheng, J. Xiao, Mussel-inspired surface immobilization of heparin on magnetic nanoparticles for enhanced wound repair via sustained release of a growth factor and M2 macrophage polarization, ACS Appl. Mater. Interfaces 13 (2) (2021) 2230–2244.
[45] Y. Wang, Z. Lyu, Y. Qin, X. Wang, L. Sun, Y. Zhang, L. Gong, S. Wu, S. Han, Y. Tang, Y. Jia, D.L. Kwong, N. Kam, X.Y. Guan, FOXO1 promotes tumor progression by increased M2 macrophage infiltration in esophageal squamous cell carcinoma, Theranostics 10 (25) (2020) 11535–11548.
[46] K.D. Hankenson, K. Gagne, M. Shaughnessy, Extracellular signaling molecules to promote fracture healing and bone regeneration, Adv. Drug Deliv. Rev. 94 (2015) 3–12.
[47] K. Hu, B.R. Olsen, Osteoblast-derived VEGF regulates osteoblast differentiation and bone formation during bone repair, J. Clin. Invest. 126 (2) (2016) 509–526.
[48] J. Yang, Y. Zhou, F. Wei, Y. Xiao, Blood clot formed on rough titanium surface induces early cell recruitment, Clin. Oral Implants Res. 27 (8) (2016) 1031–1038.
[49] A.M. Bohm, N. Dirckx, R.J. Tower, N. Peredo, S. Vanuytven, K. Theunis, E. Nefyodova, R. Cardoen, V. Lindner, T. Voet, M. Van Hul, C. Maes, Activation of skeletal stem and progenitor cells for bone regeneration is driven by PDGFRbeta signaling, Dev. Cell 51 (2) (2019) 236–254 e12.
[50] Y. Xu, K. Cui, J. Li, X. Tang, J. Lin, X. Lu, R. Huang, B. Yang, Y. Shi, D. Ye, J. Huang, S. Yu, X. Liang, Melatonin attenuates choroidal neovascularization by regulating macrophage/microglia polarization via inhibition of RhoA/ROCK signaling pathway, J. Pineal Res. 69 (1) (2020), e12660.
[51] K. Van Raemdonck, S. Umar, K. Palasiewicz, S. Volkov, M.V. Volin, S. Arami, H. J. Chang, B. Zanotti, N. Sweiss, S. Shahrara, CCL21/CCR7 signaling in macrophages promotes joint inflammation and Th17-mediated osteoclast formation in rheumatoid arthritis, Cell. Mol. Life Sci. 77 (7) (2020) 1387–1399.
[52] F. Cruz-Guilloty, A.M. Saeed, S. Duffort, M. Cano, K.B. Ebrahimi, A. Ballmick, Y. Tan, H. Wang, J.M. Laird, R.G. Salomon, J.T. Handa, V.L. Perez, T cells and macrophages responding to oxidative damage cooperate in pathogenesis of a mouse model of age-related macular degeneration, PloS One 9 (2) (2014), e88201.
[53] A.K. Jha, S.C. Huang, A. Sergushichev, V. Lampropoulou, Y. Ivanova, E. Loginicheva, K. Chmielewski, K.M. Stewart, J. Ashall, B. Everts, E.J. Pearce, E. M. Driggers, M.N. Artyomov, Network integration of parallel metabolic and transcriptional data reveals metabolic modules that regulate macrophage polarization, Immunity 42 (3) (2015) 419–430.
[54] Z. Khan, D.Y. Cao, J.F. Giani, E.A. Bernstein, L.C. Veiras, S. Fuchs, Y. Wang, Z. Peng, M. Kalkum, G.Y. Liu, K.E. Bernstein, Overexpression of the C-domain of angiotensin-converting enzyme reduces melanoma growth by stimulating M1 macrophage polarization, J. Biol. Chem. 294 (12) (2019) 4368–4380.
[55] M.A. El Azreq, C. Arseneault, M. Boisvert, N. Page, I. Allaeys, P.E. Poubelle, P. A. Tessier, F. Aoudjit, Cooperation between IL-7 receptor and integrin alpha2beta1 (CD49b) drives Th17-mediated bone loss, J. Immunol. 195 (9) (2015) 4198–4209.
[56] X.Q. Huang, X. Cen, W.T. Sun, K. Xia, L.Y. Yu, J. Liu, Z.H. Zhao, CircPOMT1 and circMCM3AP inhibit osteogenic differentiation of human adipose-derived stem cells by targeting miR-6881-3p, Am. J. Transl. Res. 11 (8) (2019) 4776–4788.
[57] T. Kawamura, Y. Ogawa, O. Shimozato, T. Ando, A. Nakao, T. Kobata, K. Okumura, H. Yagita, S. Shimada, CD70 is selectively expressed on Th1 but not on Th2 cells and is required for Th1-type immune responses, J. Invest. Dermatol. 131 (6) (2011) 1252–1261.
[58] J. Song, B. Ye, H. Liu, R. Bi, N. Zhang, J. Hu, E. Luo, Fak-Mapk, Hippo and Wnt signalling pathway expression and regulation in distraction osteogenesis, Cell Prolif 51 (4) (2018), e12453.
[59] F. Loi, L.A. Cordova, R. Zhang, J. Pajarinen, T.H. Lin, S.B. Goodman, Z. Yao, The effects of immunomodulation by macrophage subsets on osteogenesis in vitro, Stem Cell Res. Ther. 7 (2016) 15.
[60] S. Lotinun, R. Kiviranta, T. Matsubara, J.A. Alzate, L. Neff, A. Luth, I. Koskivirta, B. Kleuser, J. Vacher, E. Vuorio, W.C. Horne, R. Baron, Osteoclast-specific cathepsin K deletion stimulates S1P-dependent bone formation, J. Clin. Invest. 123 (2) (2013) 666–681.
[61] L. Pederson, M. Ruan, J.J. Westendorf, S. Khosla, M.J. Oursler, Regulation of bone formation by osteoclasts involves Wnt/BMP signaling and the chemokine sphingosine-1-phosphate, Proc. Natl. Acad. Sci. U. S. A. 105 (52) (2008) 20764–20769.
[62] E.C. Walker, N.E. McGregor, I.J. Poulton, S. Pompolo, E.H. Allan, J.M. Quinn, M. T. Gillespie, T.J. Martin, N.A. Sims, Cardiotrophin-1 is an osteoclast-derived stimulus of bone formation required for normal bone remodeling, J. Bone Miner. Res. 23 (12) (2008) 2025–2032.
[63] S. Takeshita, T. Fumoto, K. Matsuoka, K.A. Park, H. Aburatani, S. Kato, M. Ito, K. Ikeda, Osteoclast-secreted CTHRC1 in the coupling of bone resorption to formation, J. Clin. Invest. 123 (9) (2013) 3914–3924.
[64] A. Teti, Mechanisms of osteoclast-dependent bone formation, BoneKEy Rep. 2 (2013) 449.
[65] B.J. Kim, Y.S. Lee, S.Y. Lee, W.Y. Baek, Y.J. Choi, S.A. Moon, S.H. Lee, J.E. Kim, E. J. Chang, E.Y. Kim, J. Yoon, S.W. Kim, S.H. Ryu, S.K. Lee, J.A. Lorenzo, S.H. Ahn, H. Kim, K.U. Lee, G.S. Kim, J.M. Koh, Osteoclast-secreted SLIT3 coordinates bone resorption and formation, J. Clin. Invest. 128 (4) (2018) 1429–1441.
[66] M. Grano, F. Galimi, G. Zambonin, S. Colucci, E. Cottone, A.Z. Zallone, P. M. Comoglio, Hepatocyte growth factor is a coupling factor for osteoclasts and osteoblasts in vitro, Proc. Natl. Acad. Sci. U. S. A. 93 (15) (1996) 7644–7648.
[67] T. Negishi-Koga, M. Shinohara, N. Komatsu, H. Bito, T. Kodama, R.H. Friedel, H. Takayanagi, Suppression of bone formation by osteoclastic expression of semaphorin 4D, Nat. Med. 17 (11) (2011) 1473–1480.
[68] N. Kusu, J. Laurikkala, M. Imanishi, H. Usui, M. Konishi, A. Miyake, I. Thesleff, N. Itoh, Sclerostin is a novel secreted osteoclast-derived bone morphogenetic protein antagonist with unique ligand specificity, J. Biol. Chem. 278 (26) (2003) 24113–24117.